Available online at www.sciencedirect.com
ScienceDirect
Trans. Nonferrous Met. Soc. China 34(2024) 3002−3015
Transactions of Nonferrous Metals Society of China
www.tnmsc.cn

A novel surfactant *N*-hydroxy-9,10-epoxy group-octadecanamide: Part II. Its synthesis and application in flotation separation of spodumene and albite

Wei-di ZHANG[1,2,3,4], Meng-jie TIAN[1,2,3,4], Wei SUN[1,2]

1. School of Minerals Processing and Bioengineering, Central South University, Changsha 410083, China;
2. State Key Laboratory of Mineral Processing, Beijing 102600, China;
3. Hubei Key Laboratory for Efficient Utilization and Agglomeration of Metallurgic Mineral Resources, Wuhan 430081, China;
4. Key Laboratory of Hunan Province for Clean and Efficient Utilization of Strategic Calcium-containing Mineral Resources, Central South University, Changsha 410083, China

Received 6 March 2023; accepted 20 September 2023

Abstract: A novel hydroxamic acid, *N*-hydroxy-9,10-epoxy group-octadecanamide (*N*-OH-9,10-O-ODA), was synthesised by modifying the structure of oleic acid. The carboxyl group of oleic acid was converted into an *N*-hydroxy amide group, and an epoxy group was introduced into its structure. *N*-OH-9,10-O-ODA was used as a novel collector in the flotation separation of spodumene from one of its associated gangue minerals, specifically albite. *N*-OH-9,10-O-ODA exhibits remarkable selectivity, with a stronger affinity for collecting spodumene particles compared to albite particles. Zeta potential measurements and X-ray photoelectron spectroscopic analysis reveal that the adsorption quantity of *N*-OH-9,10-O-ODA on spodumene surface is comparable to that on albite surface. First-principles calculations demonstrate the diverse adsorption configurations of *N*-OH-9,10-O-ODA on surfaces of spodumene and albite, leading to its distinct collecting abilities for spodumene and albite particles.

Key words: *N*-hydroxy-9,10-epoxy group-octadecanamide; spodumene; albite; flotation separation; oleic acid

1 Introduction

Lithium (Li) is extensively applied in the industrial applications, including ceramics and electronics [1]. Li-ion batteries find widespread usage in electric appliances and power tools [2−4]. Research on Li-ion batteries is rapidly advancing due to the increasing demand driven by portable electronics and new energy vehicles [5].

Spodumene, an important Li-containing mineral, often coexists with other silicate minerals including albite ($NaAlSi_3O_8$) and quartz [6]. The prior separation of spodumene and its associated gangue minerals is necessary to reduce the cost of Li extraction [7−9]. Flotation plays a significant role in recovering fine-grained spodumene and separating spodumene from gangue minerals [10−12]. In spodumene flotation, collectors, such as hydroxamic acids, fatty acids, and amines, are used to selectively enhance the hydrophobicity of target minerals [13−15].

Hydroxamic acids exhibit exceptional selectivity in oxide mineral flotations due to their high electronegativities and reactivities with metal ions on mineral surfaces [16−19]. Salicylhydroxamic

Corresponding author: Meng-jie TIAN, Tel: +86-17866828110, E-mail: mengjietian@csu.edu.cn
DOI: 10.1016/S1003-6326(24)66591-X

acid (SHA) is a widely utilised collector for oxide minerals, including spodumene [20−22]. While SHA exhibits excellent selectivity, its collection capacity is limited. Divalent lead ions (Pb^{2+}) are commonly used activators to enhance the collecting ability of SHA [23]. Pb^{2+} ions can be adsorbed onto mineral surfaces, providing reactive sites for the subsequent adsorption of collectors [24−26]. Nonetheless, using Pb^{2+} ions is environmentally polluting and expensive [18]. Hydroxamic acids frequently serve as auxiliary collectors, facilitating the adsorption of fatty acid collectors and enhancing the selectivities of the reagent systems [27].

In spodumene flotation, oleic acid is the most commonly used fatty acid collector due to its strong collecting ability and cost-effectiveness [28]. However, it lacks selectivity [29]. The separation of spodumene from albite necessitates collectors with high selectivities. Ca^{2+} ions are commonly employed as an activator to augment the collecting abilities of fatty acid collectors. Ca^{2+} ion adsorption exhibits non-selectivity on spodumene and gangue mineral surfaces [30]. Reagent systems employing fatty acids alone demonstrate better selectivities than those incorporating Ca^{2+} ions as an activator and fatty acids as collectors. Sodium carbonate (Na_2CO_3) can be combined with Ca^{2+} ions in spodumene flotation to inhibit the gangue minerals [31]. The interaction between CO_3^{2-} and Ca^{2+} leads to the precipitation of calcium carbonate ($CaCO_3$), effectively covering reactive sites on the gangue mineral surfaces and augmenting their hydrophilicities [32−34]. The combination of fatty acids, Ca^{2+} ions, and Na_2CO_3 enhances the surface hydrophobicity of spodumene relative to the gangue minerals.

Amines, as cationic collectors, find common usage in the flotation of aluminosilicate minerals like spodumene. The breaking of Li—O and Al—O bonds on spodumene surfaces exposes unsaturated Al^{3+} and O^{2-} ions. Spodumene surfaces become electronegative, allowing amine cations to adsorb through electrostatic attraction [35]. Dodecylamine (DDA) is a traditional amine collector in spodumene flotation, attaching to spodumene surfaces through electrostatic attraction, hydrogen bonding, and hydrophobic association. However, DDA lacks sufficient selectivity, requiring the addition of depressants to improve selectivity. Inorganic depressants have the disadvantage of environmental pollution. Sodium alginate offers an environmentally friendly alternative to inorganic depressants as an organic depressant [36,37]. It adsorbs onto mineral surfaces, hindering the subsequent adsorption of DDA on the gangue minerals associated with spodumene.

The authors [38] previously synthesized a novel hydroxamic acid collector, *N*-hydroxy-9-octadecenamide, which exhibits favorable selectivity in the flotation separation of spodumene and albite. However, it exhibits low solubility in water. To overcome this limitation, an epoxy group was introduced to the molecular structure of *N*-hydroxy-9-octadecenamide, leading to the synthesis of a novel hydroxamic acid collector known as *N*-hydroxy-9,10-epoxy group-octadecanamide (*N*-OH-9,10-O-ODA) [39]. Single mineral flotation experiments were performed to investigate the selectivity of *N*-OH-9,10-O-ODA in the flotation separation of spodumene and albite. The adsorption behaviours of *N*-OH-9,10-O-ODA on the mineral surfaces were examined through zeta potential measurements, infrared spectroscopy, X-ray photoelectron spectroscopy, and first-principles calculations. The selectivity observed in the flotation separation of spodumene and albite was elucidated based on the disparities in the adsorption behaviours of *N*-OH-9,10-O-ODA on the surfaces of the two minerals.

2 Experimental

2.1 Materials

Initially, bulk samples of spodumene and albite were ground, and the resulting mineral particles were subsequently screened to obtain samples of different sizes. Mineral particles ranging from 75 to 38 μm in size were used for flotation experiments, while particles smaller than 5 μm were employed for zeta potential measurements, infrared (IR) spectroscopic tests, and X-ray photoelectron spectroscopic (XPS) experiments.

Dilute solutions of hydrochloric acid (HCl) and sodium hydroxide (NaOH) were used as the pH regulators in the flotation experiments. Collectors employed in the flotation experiments included *N*-hydroxy-9,10-epoxy group-octadecanamide (*N*-OH-9,10-O-ODA) and oleic acid, while terpineol was used as the frother. All the reagents, except for *N*-OH-9,10-O-ODA, were supplied by

Shanghai Macklin Biochemical Co., Ltd. Sodium hydroxide and oleic acid were of analytical grade, while terpineol was of technical grade. *N*-OH-9, 10-O-ODA was synthesized in our laboratory using oleic acid as the substrate, and the supplementary materials of this paper provide comprehensive information on its synthesis method.

2.2 Flotation experiment

The flotation experiments were conducted using an XFG-II flotation device. A mineral particle suspension was prepared by mixing 2 g of mineral particles with 35 mL of deionised water at a stirring speed of 1680 r/min. The pH of the suspension was adjusted by using the pH regulators. After the addition of Ca^{2+} ion activator, the suspension was stirred for 3 min. Subsequently, it was conditioned for 3 min with either *N*-hydroxy-9,10-epoxy group-octadecanamide or oleic acid collector, followed by 1 min of conditioning with terpineol frother. The floating particles were collected over a period of 3 min, while non-floating particles were obtained by filtering the suspension after the flotation experiments. The mineral recovery was calculated based on the mass distribution between the floating and non-floating particles.

2.3 Zeta potential measurement

The zeta potential measurements were performed using a Malvern Zetasizer Nano ZS instrument. Mineral particles (35 mg) were added to 35 mL of deionised water and stirred to create a mineral particle suspension. The suspension was then conditioned for 12 min with the flotation reagents under agitation. After agitation, the suspension was left to stand for 10 min. The supernatant was collected for the zeta potential measurements. Each experiment was repeated three times.

2.4 IR spectroscopic experiment

The IR spectroscopic tests were conducted using an IRAffinity-1 spectrometer. Mineral particles (2 g) were added to 35 mL of deionised water. The resulting mixture was agitated to create the mineral particle suspension. After adding the flotation reagents, the suspension was stirred for 2 h. Subsequently, the reagent-treated mineral particles were obtained. The reagent-treated mineral particles were rinsed three times with deionised water and then dried at 45 °C. The dried product was kept for the IR spectroscopic experiments.

2.5 XPS experiment

The XPS experiments were performed by a Thermo Scientific K_α X-ray photoelectron spectrometer. The samples for the XPS experiments were prepared following the same procedure as for the IR experiments.

2.6 First-principles calculations

First-principles calculations were employed to determine the adsorption energies and optimise the adsorption configurations of *N*-OH-9,10-O-ODA on surfaces of spodumene and albite. The first-principles calculations were performed using VASP software. The computational details are provided in the supplementary materials.

According to the literature [40], the (110) surface is the predominant exposed surface of spodumene, while the (001) surface is the predominant exposed surface of albite. Therefore, the spodumene (110) surface and the albite (001) surface were chosen as the surfaces of interest for this study. The supplementary materials provide a detailed description of the construction process of the surface models of spodumene and albite.

3 Results

3.1 Flotation

Figure 1(a) illustrates the impacts of $CaCl_2$ dosage on the recoveries of spodumene and albite. The recovery of spodumene exhibits a steep rise from approximately 30% to about 60% as the $CaCl_2$ dosage increases from 0 to 40 mg/L. Subsequently, it gradually increases to around 80% with a further increase in the $CaCl_2$ dosage to 120 mg/L, while using *N*-OH-9,10-O-ODA and terpineol at dosages of 6.0×10^{-4} mol/L and 7.71 mg/L, respectively, and maintaining the pH values of the suspensions of spodumene particles at 10. The recovery of spodumene remains steady at approximately 80% when the $CaCl_2$ dosage exceeds 120 mg/L. Conversely, the recovery of albite gradually increases from around 10% to about 50% with an increase in the $CaCl_2$ dosage from 0 to 200 mg/L. The utilization of *N*-OH-9,10-O-ODA as the collector results in higher recoveries of spodumene compared to albite, exhibiting a difference of

30%−50% within the investigated $CaCl_2$ dosage range.

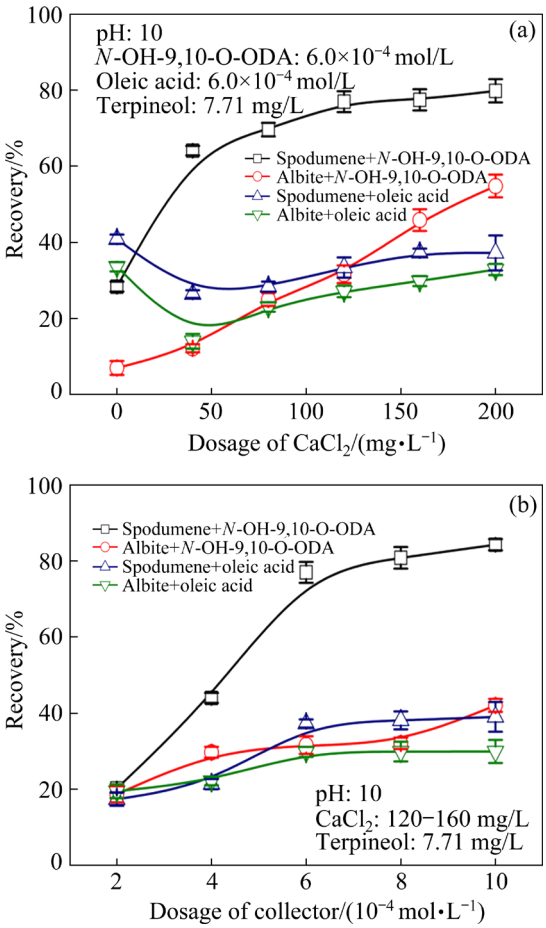

Fig. 1 Recoveries of spodumene and albite as function of dosages of $CaCl_2$ (a) and collector (b)

The recovery of spodumene exhibits a similar trend to that of albite when using oleic acid as the collector. The recovery of spodumene decreases from approximately 40% to around 30% as the $CaCl_2$ dosage increases from 0 to 40 mg/L. Subsequently, it gradually increases to about 40% with a further increase in the $CaCl_2$ dosage to 120 mg/L, while maintaining oleic acid and terpineol dosages of 6.0×10^{-4} mol/L and 7.71 mg/L, respectively, and the pH values of the suspensions of albite particles at 10. The recovery of spodumene remains stable at approximately 40% when the $CaCl_2$ dosage exceeds 120 mg/L. Conversely, the recovery of albite gradually decreases from around 30% to about 10% as the $CaCl_2$ dosage increases from 0 to 40 mg/L, and then slowly increases to approximately 40% with a further increase in the $CaCl_2$ dosage to 200 mg/L. The use of oleic acid as the collector results in higher recoveries of spodumene compared to albite, with a maximum difference of approximately 10% between the two.

Figure 1(b) shows the impacts of *N*-OH-9,10-O-ODA and oleic acid dosages on the recoveries of spodumene and albite. With an increase in the *N*-OH-9,10-O-ODA dosage from 2.0×10^{-4} to 6.0×10^{-4} mol/L, the recovery of spodumene increases from approximately 20% to around 80% and subsequently maintains a constant value of around 80% as the *N*-OH-9,10-O-ODA dosage continues to increase. Conversely, the recovery of albite exhibits a gradual increase from approximately 20% to around 30% as the *N*-OH-9,10-O-ODA dosage increases from 2.0×10^{-4} to 6.0×10^{-4} mol/L. It subsequently maintains a constant value of around 30% with further increase in the *N*-OH-9,10-O-ODA dosage. Spodumene particles treated with *N*-OH-9,10-O-ODA exhibit higher recoveries compared to albite particles treated with *N*-OH-9,10-O-ODA, resulting in a difference of 50% between the two within the *N*-OH-9,10-O-ODA dosage range from 6.0×10^{-4} to 1.0×10^{-3} mol/L.

The recovery of spodumene exhibits a similar trend to that of albite when using oleic acid as the collector, in terms of the variation with oleic acid dosage. The recovery of spodumene gradually increases from approximately 20% to around 40% when an increase in the oleic acid dosage from 2.0×10^{-4} to 6.0×10^{-4} mol/L. It subsequently stabilizes at around 40% with further increase in the oleic acid dosage. Conversely, the recovery of albite exhibits an increase from about 20% to around 30% as the oleic acid dosage increases from 2.0×10^{-4} to 6.0×10^{-4} mol/L. It subsequently stabilizes at approximately 30% with further increase in the oleic acid dosage. Spodumene particles treated with oleic acid exhibit higher recoveries compared to albite particles treated with oleic acid, resulting in a difference of about 10% between the two within the oleic acid dosage range from 6.0×10^{-4} to 1.0×10^{-3} mol/L.

3.2 Zeta potential

Figure 2 illustrates the zeta potentials of spodumene and albite as a function of the pH value of the suspensions of the mineral particles. The zeta potentials of spodumene and albite surfaces exhibit a negative correlation with the pH. The treatments of Ca^{2+} with spodumene and albite surfaces result in

higher zeta potentials compared to pure spodumene and albite surfaces. The treatment of Ca^{2+} results in comparable increase in the zeta potentials of both spodumene and albite, by approximately 40 mV. The inclusion of *N*-OH-9,10-O-ODA leads to a decrease of around 20 mV in the zeta potential of the Ca^{2+}-treated spodumene surface, a reduction comparable to that observed in the zeta potential of the Ca^{2+}-treated albite surface upon the inclusion of *N*-OH-9,10-O-ODA within the pH range of 8−11.

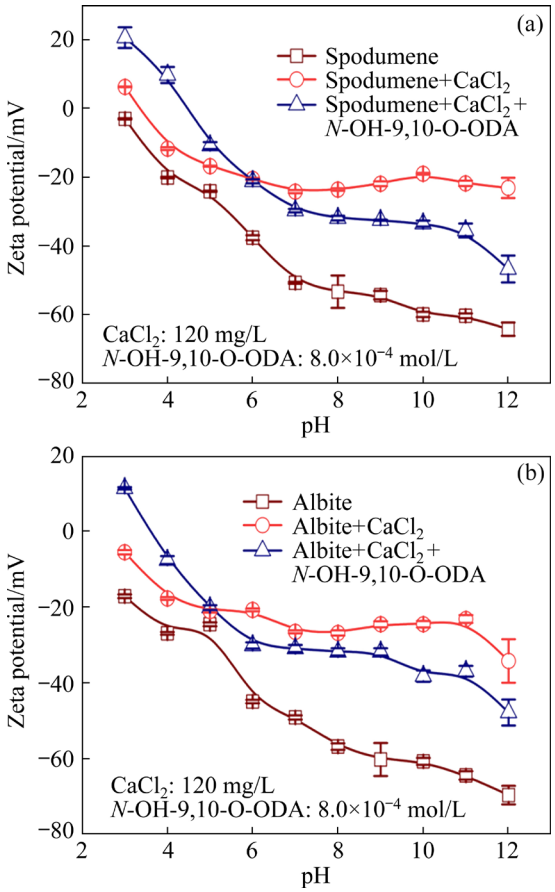

Fig. 2 Zeta potentials of spodumene (a) and albite (b) surfaces as function of pH

3.3 Infrared (IR) spectra

Figure 3(a) displays the IR spectra of untreated and flotation reagent-treated spodumene particles. The IR spectrum of spodumene particles treated with Ca^{2+} and *N*-OH-9,10-O-ODA exhibits six distinct peaks, not observed in the spectrum of pure spodumene particles. The peaks centered at 2922.3 and 2853.8 cm^{-1} are ascribed to the —CH_2— and —CH_3 groups of *N*-OH-9,10-O-ODA [38]. The N—H group of *N*-OH-9,10-O-ODA contributes to the peak at 1601.0 cm^{-1} [41]. The peak centered at 1470.0 cm^{-1} is attributed to the carboxyl group of *N*-OH-9,10-O-ODA [42]. The peak centered at 1076.4 cm^{-1} is characteristic of the carbonyl group of *N*-OH-9,10-O-ODA [43]. The peak centered at 932.0 cm^{-1} represents the C—N group [44].

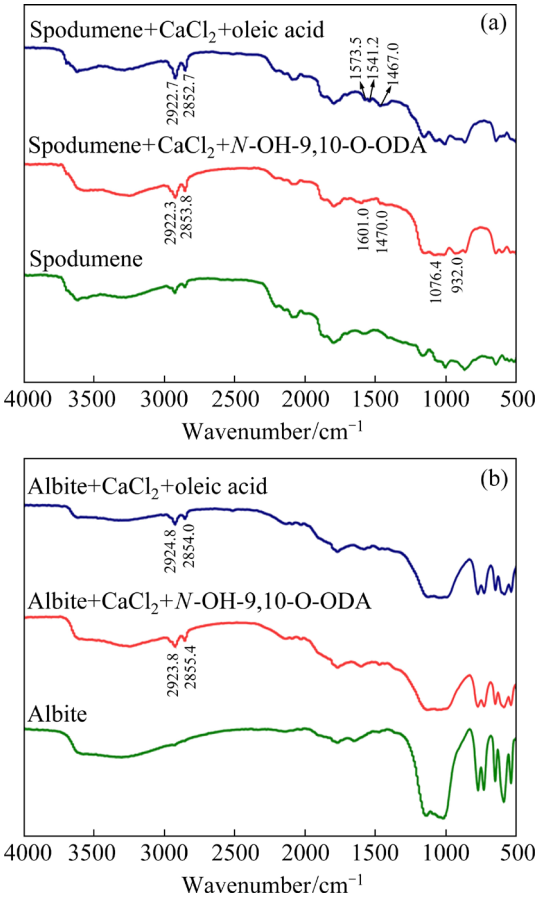

Fig. 3 IR spectra of spodumene (a) and albite (b) particles untreated and treated with flotation reagents

The IR spectrum of spodumene particles treated with Ca^{2+} and oleic acid exhibits five additional peaks compared to the spectrum of pure spodumene particles. The peaks at 2922.7 and 2852.7 cm^{-1} are attributed to the —CH_2— and —CH_3 groups of oleic acid. The peaks at 1573.5, 1541.2 and 1467.0 cm^{-1} are characteristic of the carboxyl group of oleic acid.

Figure 3(b) displays IR spectra of untreated and flotation-reagent-treated albite particles. Albite particles treated with Ca^{2+} and *N*-OH-9,10-O-ODA exhibit two distinct adsorption bands at 2923.8 and 2855.4 cm^{-1} in their IR spectrum, which correspond to the —CH_2— and —CH_3 groups of *N*-OH-9, 10-O-ODA. Albite particles treated with Ca^{2+} and oleic acid also exhibit characteristic peaks at 2924.8 and 2854.0 cm^{-1}, corresponding to the —CH_2— and —CH_3 groups of oleic acid.

3.4 X-ray photoelectron spectra (XPS)

Table 1 displays atomic contents on surfaces of spodumene and albite untreated and treated with flotation reagents. The XPS spectra of pure spodumene and albite surfaces exhibit no characteristic peaks of Ca and N, indicating the high purities of the used mineral samples. Ca^{2+}-treated spodumene and albite surfaces display characteristic peaks of Ca, indicating the adsorption of Ca^{2+} on their respective surfaces. Spodumene and albite surfaces treated with Ca^{2+} and *N*-OH-9,10-O-ODA display characteristic peaks of N, indicating the adsorption of *N*-OH-9,10-O-ODA on their respective surfaces. Spodumene surface treated with Ca^{2+} and *N*-OH-9,10-O-ODA exhibits a similar concentration of N as albite surface treated with Ca^{2+} and *N*-OH-9,10-O-ODA. Spodumene surface treated with Ca^{2+} and *N*-OH-9,10-O-ODA displays an increase of 15.60% in C concentration compared to Ca^{2+}-treated spodumene surface. Albite surface treated with Ca^{2+} and *N*-OH-9,10-O-ODA exhibits an increase of 16.65% in C concentration compared to Ca^{2+}-treated albite surface. These findings indicate that the adsorption quantities of *N*-OH-9,10-O-ODA on the Ca^{2+}-activated surfaces of spodumene and albite are comparable.

Figure 4(a) displays the high-resolution XPS spectra of Al 2p of spodumene surfaces untreated and treated with flotation reagents. The Al 2p peak in the XPS spectrum of Ca^{2+}-treated spodumene surface exhibits a binding energy similar to that of the Al 2p peak in the XPS spectrum of pure spodumene surface. This finding indicates that Al^{3+} ions on spodumene surface do not participate in the adsorption process of Ca^{2+} ions on spodumene surface. The binding energy of the Al 2p peak in the XPS spectrum of spodumene surface treated with Ca^{2+} and *N*-OH-9,10-O-ODA shows almost no change compared to those in the XPS spectra of both pure and Ca^{2+}-treated spodumene surfaces.

Figure 4(b) presents the high-resolution XPS spectra of Ca 2p of Ca^{2+}-treated spodumene surfaces. The Ca 2p band exhibits two single peaks at 348.07 and 351.62 eV in the XPS spectrum of Ca^{2+}-treated spodumene surface. In the XPS spectrum of spodumene surface treated with Ca^{2+} and *N*-OH-9,10-O-ODA, the two peaks of Ca 2p exhibit negative shifts of 0.45 and 0.43 eV in their binding energies compared to those in the spectrum of Ca^{2+}-treated spodumene surface.

Figure 4(c) displays the high-resolution XPS spectra of C 1s of both untreated and flotation-reagent-treated spodumene surfaces. The broad C 1s band consists of two single peaks at 286.56 and 284.81 eV in the XPS spectrum of pure spodumene surface. The two peaks represent carbon contamination on this surface. The intensities of the two peaks in the XPS spectrum of spodumene surface treated with Ca^{2+} and *N*-OH-9,10-O-ODA are higher than those of the peaks in the spectrum of Ca^{2+}-treated spodumene surface. An additional peak of C 1s at 288.30 eV is observed. This peak corresponds to the carbonyl group of *N*-OH-9,10-O-ODA adsorbed on spodumene surface. The increase in the intensities of the C 1s peaks and the emergence of the novel C 1s peak indicate that *N*-OH-9,10-O-ODA is adsorbed on spodumene surface.

Figure 4(d) presents the high-resolution XPS spectra of Al 2p of both untreated and flotation-reagent-treated albite surfaces. The XPS spectrum of pure albite surface displays a single peak of Al 2p at 74.28 eV. The binding energy of the Al 2p peak in the XPS spectrum of Ca^{2+}-treated albite surface is shifted negatively by 0.18 eV compared

Table 1 Atomic contents on surfaces of spodumene and albite untreated and treated with flotation reagents

Sample	Atomic content/%							
	Al 2p	C 1s	O 1s	Si 2p	Li 1s	Ca 2p	N 1s	Na 1s
Spodumene	8.62	21.67	48.00	15.65	6.06	−	−	−
Spodumene+Ca^{2+}	9.05	22.71	42.05	16.64	8.72	0.84	−	−
Spodumene+Ca^{2+}+*N*-OH-9,10-O-ODA	6.87	38.31	33.80	14.19	4.90	0.83	1.09	−
Albite	8.05	15.67	51.91	23.21	−	−	−	1.16
Albite+Ca^{2+}	7.26	12.86	50.82	21.91	5.36	0.48	−	1.31
Albite+Ca^{2+}+*N*-OH-9,10-O-ODA	6.23	29.51	42.43	18.94	−	0.44	1.13	1.33

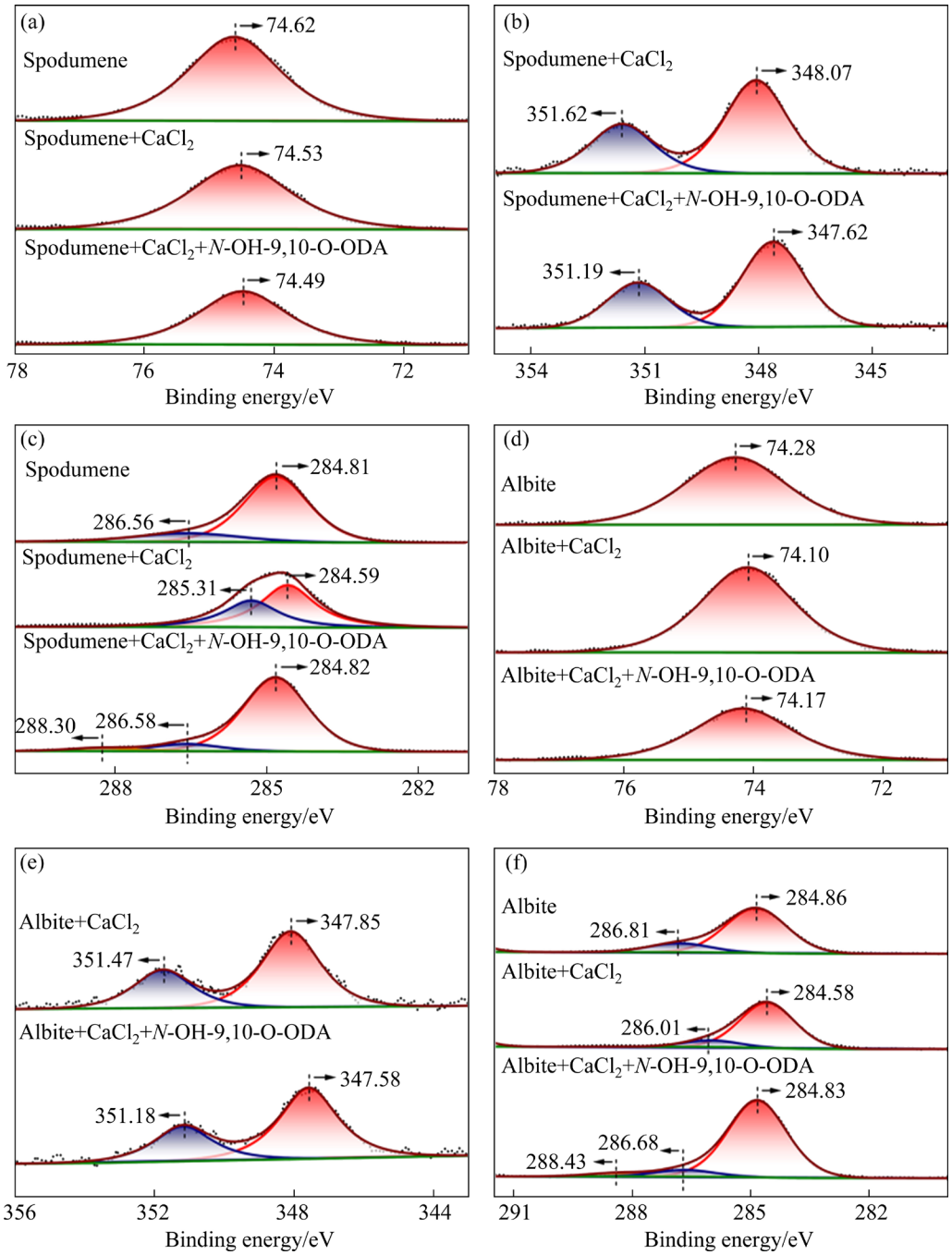

Fig. 4 High-resolution XPS spectra of Al 2p (a), Ca 2p (b) and C 1s (c) of spodumene surfaces untreated and treated with flotation reagents and those of Al 2p (d), Ca 2p (e) and C 1s (f) of albite surfaces untreated and treated with flotation reagents

to that of the peak in the spectrum of pure albite surface. The binding energy of the Al 2p peak in the XPS spectrum of albite surface treated with Ca^{2+} and *N*-OH-9,10-O-ODA is comparable to that in the spectrum of Ca^{2+}-treated albite surface.

Figure 4(e) illustrates the high-resolution XPS spectra of Ca 2p of both untreated and flotation-reagent-treated albite surfaces. The broad Ca 2p band in the XPS spectrum of Ca^{2+}-treated albite surface consists of two component peaks centered at 347.85 and 351.47 eV. The binding energies of the two Ca 2p peaks in the XPS spectrum of albite surface treated with Ca^{2+} and *N*-OH-9,10-O-ODA shift to more negative positions compared to those of the Ca 2p peaks in the XPS spectrum of Ca^{2+}-treated albite surface. The shift values range

from 0.27 to 0.29 eV.

Figure 4(f) shows the high-resolution XPS spectra of C 1s of both untreated and flotation-reagent-treated albite surfaces. The broad C 1s band in the XPS spectrum of pure albite surface is characterised by two single peaks at 284.86 and 286.81 eV. The two peaks are attributed to surface carbon contamination. The intensities of the two peaks in the XPS spectrum of albite surface treated with Ca^{2+} and *N*-OH-9,10-O-ODA are higher than those of the peaks of C 1s in the spectrum of untreated and Ca^{2+}-treated albite surfaces. This finding indicates the adsorption of *N*-OH-9,10-O-ODA on pure and Ca^{2+}-treated albite surfaces.

3.5 First-principles calculations

Figure 5(a) displays the optimised adsorption configuration of *N*-OH-9,10-O-ODA on the (110) surface of spodumene. *N*-OH-9,10-O-ODA forms two monodentate bonds with two Al^{3+} ions on pure spodumene surface through its carbonyl and *N*-bonded O atoms, having bond lengths of 2.00 and 2.08 Å, respectively. It is adsorbed on spodumene surface with an adsorption energy of −140.16 kJ/mol (Table 2). Figure 5(b) illustrates the optimised adsorption configuration of *N*-OH-9,10-O-ODA on Ca^{2+}-activated spodumene surface.

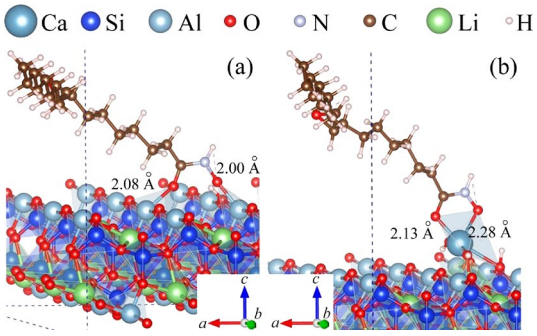

Fig. 5 Optimised adsorption configurations of *N*-OH-9,10-O-ODA on pure (a) and Ca^{2+}-activated (110) (b) surfaces of spodumene

Table 2 Adsorption energies of *N*-OH-9,10-O-ODA on (110) surface of spodumene and (001) surface of albite

Mineral surface	Adsorption energy/ (kJ·mol^{-1})
Pure spodumene	−140.16
Ca^{2+}-activated spodumene	−453.82
Pure albite (vertical model)	−425.53
Pure albite (horizontal model)	−508.09

N-OH-9,10-O-ODA forms a five-membered chelate ring with a Ca^{2+} ion adsorbed on spodumene surface, exhibiting bond lengths of 2.13 and 2.28 Å. It is adsorbed on Ca^{2+}-activated spodumene surface with an adsorption energy of −453.82 kJ/mol (Table 2).

4 Discussion

The recovery of spodumene is much higher compared to that of albite when using *N*-hydroxy-9,10-epoxy group-octadecanamide (*N*-OH-9,10-O-ODA) as the collector (Fig. 1). This flotation experimental result demonstrates the excellent selectivity of *N*-OH-9,10-O-ODA in the flotation separation of spodumene and albite. Using oleic acid as the collector results in the recovery of spodumene similar to that of albite and the lower recovery of spodumene compared to using *N*-OH-9, 10-O-ODA as the collector (Fig. 1). These results suggest that *N*-OH-9,10-O-ODA exhibits super selectivity and stronger collecting capacity compared to oleic acid.

The characteristic peaks of *N*-OH-9,10-O-ODA are observed in the IR spectra of spodumene and albite surfaces treated with Ca^{2+} and *N*-OH-9, 10-O-ODA, while the peaks of oleic acid are present in the spectra of spodumene and albite treated with Ca^{2+} and oleic acid (Fig. 3). These IR spectroscopic test results indicate the chemisorptions of *N*-OH-9,10-O-ODA and oleic acid on surfaces of spodumene and albite.

Spodumene and albite surfaces treated with Ca^{2+} ions exhibit higher zeta potentials compared to pure spodumene and albite surfaces (Fig. 2). The presence of Ca element is observed in the XPS spectra of spodumene and albite surfaces treated with Ca^{2+} ions (Table 1). The adsorption of Ca^{2+} on surfaces of spodumene and albite is supported by the combination of the zeta potential measurements and XPS tests.

Treatments of *N*-OH-9,10-O-ODA with Ca^{2+}-treated spodumene and albite surfaces lead to a comparable decrease of 20 mV in the zeta potentials of Ca^{2+}-treated spodumene and albite surfaces (Fig. 2). Furthermore, it results in a comparable increase of 15.60% in C concentration on Ca^{2+}-treated spodumene surface to that of 16.65% in C concentration on Ca^{2+}-treated albite surface (Table 1). The spodumene surface treated with Ca^{2+}

and *N*-OH-9,10-O-ODA exhibits a similar N concentration of 1.09% to that of 1.13% observed on albite surface treated with Ca^{2+} and *N*-OH-9, 10-O-ODA (Table 1). The combination of the zeta potential measurements and XPS tests reveals that the adsorption amount of *N*-OH-9,10-O-ODA on spodumene surface is comparable to that on albite surface.

Spodumene particles exhibit higher recoveries than albite particles when *N*-OH-9,10-O-ODA is used as the collector (Fig. 1). These flotation experimental results suggest that *N*-OH-9,10-O-ODA has a higher affinity for collecting spodumene particles compared to albite particles. It is expected that the adsorption amount of *N*-OH-9,10-O-ODA on spodumene surface would be greater than that on albite surface. However, contrary to this expectation, the combination of the zeta potential measurements and XPS tests does not indicate a noticeable difference in the adsorption amount of *N*-OH-9, 10-O-ODA between surfaces of spodumene and albite. The differing adsorption configurations of *N*-OH-9,10-O-ODA on spodumene and albite surfaces can account for the difference in its abilities to collect spodumene and albite particles [40,45]. The research findings of this paper provide insights into three factors contributing to the distinct adsorption configurations of *N*-OH-9,10-O-ODA on surfaces of spodumene and albite. Firstly, notable variations exist in the surface properties of spodumene and albite. In comparison with albite surface, spodumene surface exhibits a higher quantity of broken bonds involving Al^{3+} ions, leading to an enhanced reactivity of Al^{3+} ions on spodumene surface. Consequently, *N*-OH-9,10-O-ODA displays a greater propensity to interact with Al^{3+} ions on spodumene surface, resulting in an adsorption configuration where its carbon chain aligns perpendicularly to spodumene surface (Fig. 5(a)). Conversely, albite surface possesses a higher concentration of reactive O atoms, facilitating the formation of hydrogen bonds between *N*-OH-9,10-O-ODA and O atoms on albite surface. Consequently, *N*-OH-9,10-O-ODA adsorbs in a configuration where its carbon chain aligns parallel to albite surface (Fig. 6(b)).

N-OH-9,10-O-ODA can bridge two adjacent Al^{3+} ions on pure spodumene surface (Fig. 5(a)). It exhibits an adsorption energy of −140.16 kJ/mol on spodumene surface (Table 2). *N*-OH-9,10-O-ODA can form a five-membered chelate ring with a Ca^{2+} ion adsorbed on spodumene surface (Fig. 5(b)). It exhibits an adsorption energy of −453.82 kJ/mol on Ca^{2+}-activated spodumene surface (Table 2). Utilising Ca^{2+} ions as the activator provides additional active sites for the adsorption of *N*-OH-9, 10-O-ODA on spodumene surface and enhances the interaction strength between *N*-OH-9,10-O-ODA and spodumene surface. These optimisation results of the adsorption configurations of *N*-OH-9,10-O-ODA demonstrate that *N*-OH-9,10-O-ODA exhibits a preference for the vertical adsorption configuration on both pure and Ca^{2+}-activated spodumene surfaces, with its carbon chain perpendicular to the surfaces.

N-OH-9,10-O-ODA can form a five-membered chelate ring with a Na^+ ion on albite surface, with Na—O bond lengths of 2.25 and 2.42 Å (Fig. 6(a)). It exhibits an adsorption energy of −425.53 kJ/mol on pure albite surface (Table 2). Additionally, *N*-OH-9,10-O-ODA can adopt a vertical adsorption configuration on pure albite surface due to the interaction between its O atoms and a Na^+ ion on pure albite surface. The Na concentration on pure

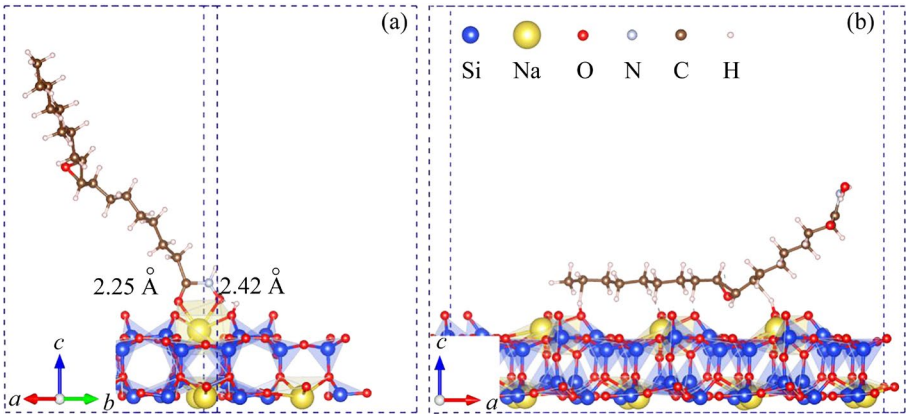

Fig. 6 Two optimised adsorption configurations of *N*-OH-9,10-O-ODA on (001) surface of albite

albite surface is 1.16%, significantly lower than the Al concentration of 8.62% on pure spodumene surface (Table 1). Pure albite surface exhibits a low concentration of Na^+ due to the high solubility of Na^+ ions on albite surface. Therefore, the vertical model is not the primary adsorption model of *N*-OH-9,10-O-ODA on albite surface.

In spodumene crystal, an Al^{3+} ion is bonded to six O^{2-} ions and is positioned at the center of an O octahedron (Fig. 7(a)) [46]. In albite crystal, Al^{3+} and Si occupy the same site [6]. An Al^{3+} ion in albite crystal forms bonds with four O^{2-} ions and is situated at the center of an O tetrahedron (Fig. 7(b)). The coordination number of Al^{3+} ions with O^{2-} ions in spodumene crystal is greater than that in albite crystal [47]. Hence, Al—O bonds in spodumene crystal are more susceptible to breakage compared to those in albite crystal. Spodumene surface exhibits a higher concentration of unsaturated Al^{3+} ions than albite surface. The majority of Al^{3+} ions on albite surface are four-coordinated and fully saturated. The number of broken bonds of unsaturated Al^{3+} ions on spodumene surface is greater than that of saturated Al^{3+} ions on albite surface, leading to an enhanced reactivity of Al^{3+} ions on spodumene surface. Direct interaction between *N*-OH-9,10-O-ODA and saturated Al^{3+} ions on albite surface is not feasible. Instead, *N*-OH-9,10-O-ODA tends to adsorb on albite surface through hydrogen bonds adopting a horizontal adsorption configuration where its carbon chain aligns parallel to albite surface (Fig. 6(b)). *N*-OH-9,10-O-ODA exhibits a higher adsorption energy of −508.09 kJ/mol in this horizontal model on albite surface compared to that of −453.82 kJ/mol on Ca^{2+}-activated spodumene surface, which indicates a strong interaction between

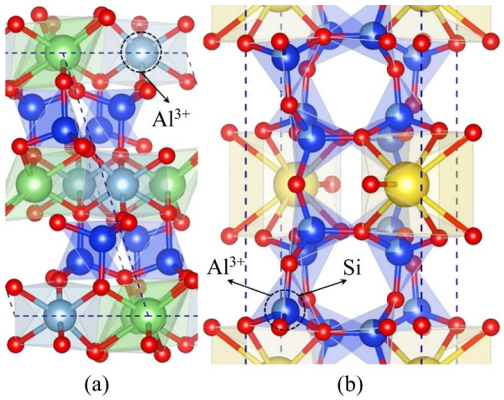

Fig. 7 Crystal structures of spodumene (a) and albite (b)

N-OH-9,10-O-ODA and O atoms on albite surface. Albite surface demonstrates a greater density of reactive O atoms than spodumene surface. The primary adsorption model of *N*-OH-9,10-O-ODA on albite surface is the horizontal model, primarily due to the strong interaction between *N*-OH-9,10-O-ODA and O atoms on albite surface, as well as the high density of O atoms on albite surface.

A vertical adsorption model of *N*-OH-9,10-O-ODA leads to the formation of patchy aggregates on spodumene surface, facilitating the attachment of bubble and the surface [40,48]. These patchy aggregates contribute to the high recovery of spodumene when *N*-OH-9,10-O-ODA is used as the collector. Conversely, the horizontal adsorption model of *N*-OH-9,10-O-ODA causes it to spread across albite surface [40]. *N*-OH-9,10-O-ODA exhibits a loose arrangement on albite surface, which hinders the attachment of bubbles and the surface. Consequently, the loose arrangement of *N*-OH-9,10-O-ODA results in a low recovery of albite when *N*-OH-9,10-O-ODA is employed as the collector.

The molecular structure of *N*-OH-9,10-O-ODA represents the second significant factor contributing to its preferential adsorption on albite surface, with its carbon chain aligning parallel to the surface. Notably, an epoxy group is situated at the middle of the long carbon chain of *N*-OH-9,10-O-ODA molecule. This epoxy group readily associates with one H^+ ion in solution, facilitating the formation of hydrogen bonds with albite surface. Consequently, the presence of this epoxy group enhances the likelihood of *N*-OH-9,10-O-ODA adsorbing on albite surface, adopting an adsorption configuration where its carbon chain is parallel to the surface.

The third determinant responsible for the varying adsorption configurations of *N*-OH-9,10-O-ODA on surfaces of spodumene and albite stems from the disparity in interaction strengths between *N*-OH-9,10-O-ODA and Ca^{2+} ions adsorbed on respective surfaces of spodumene and albite. The results from the XPS tests demonstrate that the adsorption of *N*-OH-9,10-O-ODA on spodumene surface significantly changes the binding energy of the adsorbed Ca^{2+} ions, in contrast to the change in the binding energy of the adsorbed Ca^{2+} ions on albite surface caused by the adsorption of *N*-OH-9,10-O-ODA (Figs. 4(b) and (e)). This observation

indicates a stronger interaction between *N*-OH-9,10-O-ODA and adsorbed Ca^{2+} ions on spodumene surface, rendering *N*-OH-9,10-O-ODA more inclined to interact with adsorbed Ca^{2+} ions on spodumene surface. Consequently, *N*-OH-9,10-O-ODA can more readily adsorb on spodumene surface, with its carbon chain oriented perpendicular to the surface (Fig. 5(b)).

5 Conclusions

(1) *N*-hydroxy-9,10-epoxy group-octadecanamide (*N*-OH-9,10-O-ODA) is synthesised in our laboratory and utilised as a novel flotation collector for separating spodumene from albite. The flotation experiments indicate that *N*-OH-9,10-O-ODA exhibits superior selectivity compared to oleic acid in the separation of spodumene and albite. Moreover, *N*-OH-9,10-O-ODA demonstrates a stronger capacity to collect spodumene particles than albite particles.

(2) The results from the zeta potential measurements and X-ray photoelectron spectroscopic (XPS) tests reveal a comparable adsorption quantity of *N*-OH-9,10-O-ODA on both spodumene and albite surfaces. One explanation for the disparity in the abilities of *N*-OH-9,10-O-ODA to collect spodumene and albite particles is its variable adsorption configurations on surfaces of spodumene and albite.

(3) First-principles calculations show that *N*-OH-9,10-O-ODA exhibits a preference for a vertical adsorption model on pure and Ca^{2+}-activated spodumene surfaces through chelations with Al^{3+} ions on pure spodumene surface and Ca^{2+} ions adsorbed on spodumene surface, where its carbon chain aligns perpendicularly to the surfaces. In contrast, *N*-OH-9,10-O-ODA prefers to adsorb on albite surface through hydrogen bonds in a horizontal adsorption model, with its carbon chain parallel to the surface.

(4) The vertical adsorption model of *N*-OH-9,10-O-ODA results in the formation of patchy aggregates on spodumene surface, leading to a high recovery of spodumene when *N*-OH-9,10-O-ODA is employed as the collector. The horizontal adsorption model of *N*-OH-9,10-O-ODA causes its dispersion on albite surface. *N*-OH-9,10-O-ODA assumes a loose structure on albite surface, resulting in a low recovery of albite when *N*-OH-9,10-O-ODA is used as the collector.

CRediT authorship contribution statement

Wei-di ZHANG: Investigation, Validation, Writing − Original draft; **Meng-jie TIAN:** Conceptualization, Writing – Review & editing, Funding acquisition, Supervision; **Wei SUN:** Resources, Software.

Declaration of competing interest

The authors declare that they have no known competing financial interests or personal relationships that could have appeared to influence the work reported in this paper.

Acknowledgments

The authors express their appreciation for financial support from the National Natural Science Foundation of China (Nos. 91962223, 52104287, U2067201), and Hubei Key Laboratory for Efficient Utilization and Agglomeration of Metallurgic Mineral Resources and Open Foundation of State Key Laboratory of Mineral Processing, China (No. BGRIMM-KJSKL-2022-14).

References

[1] LIU Jin-lian, YIN Zhou-lan, LI Xin-hai, HU Qi-yang, LIU Wei. Recovery of valuable metals from lepidolite by atmosphere leaching and kinetics on dissolution of lithium [J]. Transactions of Nonferrous Metals Society of China, 2019, 29(3): 641−649.

[2] NI Yang, NIE Chun-chen, SHI Shun-Xiang, ZHU Xiang-nan. Effect of mechanical force on dissociation characteristics of cathode materials in spent lithium-ion batteries [J]. Process Safety and Environmental Protection, 2022, 161: 374−383.

[3] TIAN Jia, XU Long-hua, WU Hou-qin, FANG Shuai, DENG Wei, PENG Tie-feng, SUN Wei, HU Yue-hua. A novel approach for flotation recovery of spodumene, mica and feldspar from a lithium pegmatite ore [J]. Journal of Cleaner Production, 2018, 174: 625−633.

[4] BAE J, OH S, LEE B, LEE C H, CHUNG J, KIM J, JO S, SEO S, LIM J, CHUNG S. High-performance, printable quasi-solid-state electrolytes toward all 3D direct ink writing of shape-versatile Li-ion batteries [J]. Energy Storage Materials, 2023, 57: 277−288.

[5] CAO Ning, ZHANG Ya-li, CHEN Lin-lin, JIA Yun, HUANG Yao-guo. Priority recovery of lithium and effective leaching of nickel and cobalt from spent lithium-ion battery [J]. Transactions of Nonferrous Metals Society of China, 2022, 32(5): 1677−1690.

[6] ZHOU He-peng, XIE Fan-xin, ZHANG Yong-bing, ZHANG Bo-yuan, YANG Si-qi, LUO Xian-ping. Insights into the floatability between spodumene and albite from crystal chemistry standpoint [J]. International Journal of Mining

Science and Technology, 2022, 32(6): 1329−1339.

[7] LIU Wei-jun, ZHANG Shi-qiu, WANG Wei-qing, ZHANG Jie, YAN Wu, DENG Jie, FENG Qi-ming, HUANG Yang. The effects of Ca(II) and Mg(II) ions on the flotation of spodumene using NaOL [J]. Minerals Engineering, 2015, 79: 40−46.

[8] CHU Hao-ran, CHEN Lan-lan, LU Dong-fang, WANG Yu-hua, ZHENG Xia-yu, ZHU Guang-li. Ultrasound application in alkaline pretreatment process of spodumene to improve particle floatability [J]. International Journal of Mining Science and Technology, 2023, 33: 883−891.

[9] LUO Li-ping, XU Long-hua, SHI Xin-zhang, MENG Jin-ping, LIU Ruo-hua. Microscale insights into the influence of grinding media on spodumene micro-flotation using mixed anionic/cationic collectors [J]. International Journal of Mining Science and Technology, 2022, 32(1): 171−179.

[10] HAN Wen-jie, ZHU Yi-min, GE Wen-cheng, LIU Jie, LI Yan-jun, LI Wen-bo. Flotation separation of fluorite from calcite by a new depressant curdlan and its mechanism [J]. Journal of Central South University, 2023, 30(3): 800−810.

[11] GAO Zhi-yong, JIANG Zhe-yi, SUN Wei, GAO Yue-sheng. Typical roles of metal ions in mineral flotation: A review [J]. Transactions of Nonferrous Metals Society of China, 2021, 31(7): 2081−2101.

[12] XU Yan-Ling, HUANG Kai-hua, LI Hong-qiang, HUANG Wei, LIU Cheng, YANG Si-yuan. Adsorption mechanism of styryl phosphonate ester as collector in ilmenite flotation [J]. Transactions of Nonferrous Metals Society of China, 2022, 32(12): 4088−4098.

[13] WANG Li, XU Rui, LIU Ruo-hua, GE Peng, SUN Wei, TIAN Meng-jie. Self-assembly of NaOL−DDA mixtures in aqueous solution: A molecular dynamics simulation study [J]. Molecules, 2021, 26(23): 7117.

[14] TANHUA A, SINCHE-GONZALEZ M, KALAPUDAS R, TANSKANEN P, LAMBERG P. Effect of waste rock dilution on spodumene flotation [J]. Minerals Engineering, 2020, 150: 106282.

[15] NIE Si-yue, GUO Zhi-hao, TIAN Meng-jie, SUN Wei. Selective flotation separation of cassiterite and calcite through using cinnamohydroxamic acid as the collector and Pb^{2+} as the activator [J]. Colloids and Surfaces A: Physicochemical and Engineering Aspects, 2023, 666: 131262.

[16] SARVARAMINI A, AZIZI D, LARACHI F. Hydroxamic acid interactions with solvated cerium hydroxides in the flotation of monazite and bastnasite—Experiments and DFT study [J]. Applied Surface Science, 2016, 387: 986−995.

[17] TIAN Meng-jie, HU Yue-hua, SUN Wei, LIU Run-qing. Study on the mechanism and application of a novel collector-complexes in cassiterite flotation [J]. Colloids and Surfaces A: Physicochemical and Engineering Aspects, 2017, 522: 635−641.

[18] TIAN Meng-jie, ZHANG Chen-yang, HAN Hai-sheng, LIU Run-qing, GAO Zhi-yong, CHEN Pan, WANG Li, LI Yun-zhi, JI Bin, HU Yue-hua, SUN Wei. Effects of the preassembly of benzohydroxamic acid with Fe (III) ions on its adsorption on cassiterite surface [J]. Minerals Engineering, 2018, 127: 32−41.

[19] GUO Zhi-hao, KHOSO S A, TIAN Meng-jie, SUN Wei. Utilizing *N*-hydroxy-9-octadecenamide as a collector in flotation separation of bastnaesite and fluorite [J]. Journal of Rare Earths, 2024, 42: 1620−1628.

[20] YANG Bin, CAO Shao-hang, ZHU Zhang-lei, YIN Wan-zhong, SHENG Qiu-yue, SUN Hao-ran, YAO Jin, CHEN Ke-qiang. Selective flotation separation of apatite from dolomite utilizing a novel eco-friendly and efficient depressant for sustainable manufacturing of phosphate fertilizer [J]. Journal of Cleaner Production, 2021, 286: 124949.

[21] ZHANG Shi-yong, HUANG Zhi-qiang, WANG Hong-ling, LIU Ru-kuan, CHENG Chen, GUO Zhi-qun, YU Xin-yang, HE Gui-chun, FU Weng. Separation of wolframite ore by froth flotation using a novel “crab” structure sebacoyl hydroxamic acid collector without $Pb(NO_3)_2$ activation [J]. Powder Technology, 2021, 389: 96−103.

[22] TIAN Meng-jie, GAO Zhi-yong, JI Bin, FAN Rui-ying, LIU Run-qing, CHEN Pan, SUN Wei, HU Yue-hua. Selective flotation of cassiterite from calcite with salicylhydroxamic acid collector and carboxymethyl cellulose depressant [J]. Minerals, 2018, 8(8): 316.

[23] MENG Qing-you, YUAN Zhi-tao, LI Li-xia, LU Ji-wei, YANG Jian-chao. Modification mechanism of lead ions and its response to wolframite flotation using salicylhydroxamic acid [J]. Powder Technology, 2020, 366: 477−487.

[24] TIAN Meng-jie, GAO Zhi-yong, SUN Wei, HAN Hai-sheng, SUN Lei, HU Yue-hua. Activation role of lead ions in benzohydroxamic acid flotation of oxide minerals: New perspective and new practice [J]. Journal of Colloid and Interface Science, 2018, 529: 150−160.

[25] TIAN Meng-jie, GAO Zhi-yong, HAN Hai-sheng, SUN Wei, HU Yue-hua. Improved flotation separation of cassiterite from calcite using a mixture of lead (II) ion/ benzohydroxamic acid as collector and carboxymethyl cellulose as depressant [J]. Minerals Engineering, 2017, 113: 68−70.

[26] TIAN Meng-jie, ZHANG Chen-yang, HAN Hai-sheng, LIU Run-qing, GAO Zhi-yong, CHEN Pan, HE Jian-yong, HU Yue-hua, SUN Wei, YUAN Dan-dan. Novel insights into adsorption mechanism of benzohydroxamic acid on lead (II)-activated cassiterite surface: An integrated experimental and computational study [J]. Minerals Engineering, 2018, 122: 327−338.

[27] XU Yuan-kai, YUAN Zhi-tao, MENG Qing-you, ZHAO Xuan, DU Yu-sheng. Study on the flotation behavior and interaction mechanism of ilmenite with mixed BHA/NaOL collector [J]. Minerals Engineering, 2021, 170: 107034.

[28] ZHU Guang-li, WANG Yu-hua, WANG Xu-ming, YU Fu-shun, MILLER J D. States of coadsorption for oleate and dodecylamine at selected spodumene surfaces [J]. Colloids and Surfaces A: Physicochemical and Engineering Aspects, 2018, 558: 313−321.

[29] PAN Zu-chao, ZHANG Yi-sheng, HU Jun-jie, JIAO Fen, QIN Wen-qing. Camphor leaf extract as neoteric and environmentally friendly depressant in flotation separation of scheelite and calcite [J]. Transactions of Nonferrous Metals Society of China, 2023, 33(1): 275−284.

[30] WANG Yu-hua, YU Fu-shun. Effects of metallic ions on the flotation of spodumene and beryl [J]. Journal of China University of Mining and Technology, 2007, 17(1): 35−39.

[31] WANG Li, LIU Run-qing, HU Yue-hua, LIU Jia-peng, SUN Wei. Adsorption behavior of mixed cationic/anionic surfactants and their depression mechanism on the flotation of quartz [J]. Powder Technology, 2016, 302: 15−20.

[32] RAHIMI S, IRANNAJAD M, MEHDILO A. Effects of sodium carbonate and calcium chloride on calcite depression in cationic flotation of pyrolusite [J]. Transactions of Nonferrous Metals Society of China, 2017, 27(8): 1831−1840.

[33] WILSON M, RIBEIRO M C C, WILDING M C, BENMORE C, WEBER J K R, ALDERMAN O, TAMALONIS A, PARISE J B. Structure and liquid fragility in sodium carbonate [J]. The Journal of Physical Chemistry A, 2018, 122(4): 1071−1076.

[34] CAO Miao, BU Hao, LI Shuang-ke, MENG Qing-bo, GAO Yu-de, OU Le-ming. Impact of differing water hardness on the spodumene flotation [J]. Minerals Engineering, 2021, 172: 107159.

[35] XU Long-hua, PENG Tie-feng, TIAN Jia, LU Zhong-yuan, HU Yue-hua, SUN Wei. Anisotropic surface physicochemical properties of spodumene and albite crystals: Implications for flotation separation [J]. Applied Surface Science, 2017, 426: 1005−1022.

[36] TABELIN C B, DALLAS J, CASANOVA S, PELECH T, BOURNIVAL G, SAYDAM S, CANBULAT I. Towards a low-carbon society: A review of lithium resource availability, challenges and innovations in mining, extraction and recycling, and future perspectives [J]. Minerals Engineering, 2021, 163: 106743.

[37] SHU Kai-qian, XU Long-hua, WU Hou-qin, TANG Zhen, LUO Li-ping, YANG Jie, XU Yan-bo, FENG Bo. Selective flotation separation of spodumene from feldspar using sodium alginate as an organic depressant [J]. Separation and Purification Technology, 2020, 248: 117122.

[38] ZHANG Wei-di, GUO Zhi-hao, LYU Fei, SUN Wei, GAO Zhi-yong, TIAN Meng-jie. Enhanced flotation separation of spodumene and albite via selective adsorption of *N*-hydroxy-9-octadecenamide on the mineral surfaces [J]. Minerals Engineering, 2023, 199: 108117.

[39] GUO Zhi-hao, TIAN Meng-jie, GAO Zhi-yong, SUN Wei. A novel surfactant *N*-hydroxy-9,10-epoxy group-octadecanamide. Part I. Application in the flotation separation of fluorite/calcite and adsorption selectivity on the mineral surfaces [J]. Journal of Molecular Liquids, 2023, 387: 122563.

[40] TIAN Meng-jie, GAO Zhi-yong, KHOSO S A, SUN Wei, HU Yue-hua. Understanding the activation mechanism of Pb^{2+} ion in benzohydroxamic acid flotation of spodumene: Experimental findings and DFT simulations [J]. Minerals Engineering, 2019, 143: 106006.

[41] SONG Chun-feng, LI Run, FAN Zhi-chao, LIU Qing-ling, ZHANG Bing, KITAMURA Y. CO_2/N_2 separation performance of Pebax/MIL-101 and Pebax /NH_2-MIL-101 mixed matrix membranes and intensification via sub-ambient operation [J]. Separation and Purification Technology, 2020, 238: 116500.

[42] GUO Zhi-hao, KHOSO S A, WANG Jing-gang, ZHANG Chen-yang, GAO Zhi-yong, SUN Wei, TIAN Meng-jie, LIU Yu-ling. Interaction mechanism of 2-hydroxy-3-naphthyl hydroxamic acid and 1-hydroxy-2-naphthyl hydroxamic acid in the flotation separation of bastnaesite/fluorite: Experiments and first-principles calculations [J]. Separation and Purification Technology, 2022, 285: 120307.

[43] GUO Zhi-hao, TIAN Meng-jie, QIAN Gong-ming, ZHOU You, GAO Zhi-yong, SUN Wei. Flotation separation of bastnaesite and fluorite using styrylphosphonic acid and cinnamohydroxamic acid as collectors [J]. Journal of Molecular Liquids, 2022, 362: 119766.

[44] DHAKAL T R, MISHRA S R, GLENN Z, RAI B K. Synergistic effect of PVP and PEG on the behavior of silver nanoparticle-polymer composites [J]. Journal of Nanoscience and Nanotechnology, 2012, 12(8): 6389−6396.

[45] XIE Rui-qi, ZHU Yi-min, LIU Jie, LI Yan-jun. The flotation behavior and adsorption mechanism of a new cationic collector on the separation of spodumene from feldspar and quartz [J]. Separation and Purification Technology, 2021, 264: 118445.

[46] PAGLIAI M, MUNIZ-MIRANDA M, CARDINI G, SCHETTINO V. Raman and infrared spectra of minerals from ab initio molecular dynamics simulations: The spodumene crystal [J]. Journal of Molecular Structure, 2011, 993(1/2/3): 151−154.

[47] GAO Zhi-yong, FAN Rui-ying, RALSTON J, SUN Wei, HU Yue-hua. Surface broken bonds: An efficient way to assess the surface behaviour of fluorite [J]. Minerals Engineering, 2019, 130: 15−23.

[48] LONG Xian-hao, CHEN Jian-hua, CHEN Ye. Adsorption of ethyl xanthate on ZnS(110) surface in the presence of water molecules: A DFT study [J]. Applied Surface Science, 2016, 370: 11−18.

一种新型表面活性剂 *N*-羟基-9,10-环氧基十八烷基酰胺：(II)合成及其在锂辉石/钠长石浮选分离中的应用

张伟迪[1,2,3,4]，田孟杰[1,2,3,4]，孙 伟[1,2]

1. 中南大学 资源加工与生物学院，长沙 410083；
2. 矿物加工科学与技术国家重点实验，北京 102600；
3. 冶金矿产资源高效利用与造块湖北省重点实验室，武汉 430081；
4. 中南大学 战略含钙矿物资源清洁高效利用湖南省重点实验室，长沙 410083

摘 要：使用油酸作为反应底物，其羧基转化为 *N*-羟基酰胺基，并在其结构中引入环氧基，合成一种新型羟肟酸类捕收剂 *N*-羟基-9,10-环氧基十八烷基酰胺(*N*-OH-9, 10-O-ODA)，并将其作为一种新型捕收剂应用于锂辉石与其伴生脉石矿物钠长石的浮选分离。*N*-OH-9,10-O-ODA 表现出优异的选择性，其对锂辉石颗粒的捕收能力强于钠长石颗粒。动电位测量和 X 射线光电子能谱分析结果表明，*N*-OH-9,10-O-ODA 在锂辉石表面的吸附量与其在钠长石表面的吸附量接近。第一性原理计算发现 *N*-OH-9,10-O-ODA 在锂辉石和钠长石表面存在不同的吸附构型，这导致 *N*-OH-9,10-O-ODA 对锂辉石和钠长石颗粒的浮选捕收剂能力不同。

关键词：*N*-羟基-9,10-环氧基十八烷基酰胺；锂辉石；钠长石；浮选分离；油酸

(Edited by Xiang-qun LI)